RSC Advances

ROYAL SOCIETY OF CHEMISTRY

PAPER

View Article Online
View Journal | View Issue

Cite this: *RSC Adv.*, 2026, **16**, 22879

Circular waste valorization: humic acid adsorption onto ZnS nanoparticle-loaded biomass and conversion into nutrient-rich alginate beads

J. Balaji[a] and R. Lakshmipathy *[ab]

This study aims to investigate the adsorption of humic acid onto zinc sulphide (ZnS) nanoparticle-loaded acid-activated biomass (ZnS-AAB) and its conversion to alginate beads with the addition of K^+ and NO_3^{2-} for agricultural applications. The ZnS nanoparticles were synthesized using *Manilkara zapota* seed extract and exhibited particle sizes of less than 2 nm and a band gap of 3.16 eV. The successful incorporation of ZnS into biomass was evidenced by Fourier transform infrared (FTIR) spectroscopy, X-ray diffraction (XRD), scanning electron microscopy (SEM) and energy dispersive X-ray spectroscopy (EDX). The successful encapsulation of nutrients and ZnS nanoparticle-loaded biomass into the alginate beads was confirmed by EDX analysis. The adsorption of humic acid was optimized using the Box-Behnken design and was found to be significant, with a p-value of <0.0001 and a high F-value of 408.25. Error analysis of the isotherm and kinetic data validated the applicability of the Langmuir and pseudo second-order kinetic models with low root mean square error (RMSE) and average absolute relative error (AARE) values. The release of nutrients suggested that K^+ and NO_3^{2-} released faster than humic acid and achieved 100% release within two weeks. The release kinetics of nutrients followed zero-order and Korsmeyer–Peppas (K–P) models, which were supported by correlation coefficients and low error values. The structural stability of the beads was confirmed through a swelling index study and using FTIR and SEM techniques. The overall results suggest the sustainable and circular approach of the present study with no environmental impact.

Received 3rd February 2026
Accepted 14th April 2026

DOI: 10.1039/d6ra00928j

rsc.li/rsc-advances

Introduction

Humic acid (HA) is an important organic nutrient that supports the soil in agricultural use.[1] HA is used in many agricultural practices due to its support of soil bacteria that are present on roots. The excess use of HA leads to its release into water streams without fulfilling its actual purpose and leads to the yellowish coloration of water. The major issue with the presence of HA in water streams, especially in treated or disinfected water, is the formation of various toxic products when they come in contact with disinfectants.[2,3] Considering the potential impacts, it is desirable to eliminate the HA from water streams before they are let into the water streams. There are various techniques to eliminate HA from water sources, and adsorption is one of the economical and eco-friendly techniques that prolifically eliminates HA and provides an opportunity for its reuse.

Adsorbents such as activated carbon,[4] mesoporous carbon shells,[5] natural clay,[6] zeolites,[7] animal bones[8] and nanomaterials[9] have been explored for the removal of HA from aqueous solutions. A useful review on the removal of humic acid using various adsorbents has been reported, which provides crucial insights on various adsorbents.[10] Although adsorbents from different sources have been explored for the removal of HA, they have limitations in terms of their production, availability and reuse. Researchers always look for adsorbents that are economical and efficient. A thorough literature survey revealed only a couple of studies on the direct use of nanomaterials for the adsorption of HA from aqueous solutions. Graphene oxide was explored for the removal of HA, which exhibited an adsorption capacity of 39.3 mg g^{-1} at pH 3.[11] In another study, a copper/aluminium double hydroxide layer nano adsorbent was explored, and a high removal efficiency of 277.7 3 mg g^{-1} was observed, highlighting the excellent ability of nano-phased materials in removing HA.[9] Interestingly, one study reported ZnO and TiO_2 powder-based surface modifications on walnut shells and used them as a modified adsorbent for the removal of HA.[12] The adsorption efficiency increased with surface modifications of ZnO and TiO_2 powders; however, the powders were in the bulk phase rather than in their nanomaterial form.

[a]*Department of Chemistry, Faculty of Engineering and Technology, SRM Institute of Science and Technology, Kattankulathur, Tamil Nadu, India-603203. E-mail: lakshmir11@srmist.edu.in; Lakshmipathy.vit@gmail.com*

[b]*Directorate of Learning and Development, SRM Institute of Science and Technology, Kattankulathur, Tamil Nadu, India-603203*

Most reports on HA adsorption discuss the reuse of adsorbents for consecutive cycles and do not discuss the reuse of the adsorbed or recovered HA. Considering the importance of HA in agriculture, it is appropriate to develop a process for the reuse of the adsorbed HA from aqueous solutions. In order to achieve this process, it is crucial to select appropriate adsorbents that can synergistically enhance the overall agricultural output in addition to HA. Agro-wastes are one important source of carbon and other essential minerals, such as N and S, which could be useful in developing a suitable adsorbent through surface modifications with nanomaterials.

This study aims to investigate the green synthesis of ZnS nanomaterials using agro-waste and the loading of ZnS nanomaterials onto the surface of acid-activated biomass for the removal of HA from aqueous solutions. Further, the conversion of HA-loaded ZnS biomass into beads is explored and its ability for the controlled release of nutrients for supporting plant growth systems is investigated.

Materials and methods

Preparation of aqueous extract and biomass activation

Manilkara zapota is a commonly grown fruit in Asian countries, especially India. The seeds of the fruit are usually discarded as waste due to their bitter taste; however, they are rich in biomolecules and have been explored for their medicinal value. Considering their rich biomolecule content, *Manilkara zapota* seeds (MZS) were selected in this study to prepare an aqueous extract for ZnS nanoparticle synthesis, and the acid-activated biomass was further prepared. First, the seeds were collected from a local fruit shop, washed with running water to eliminate dust, and dried in an oven at 100 °C for 2 h. Later, the dried seeds were powdered using a conventional mixture, and to prepare the aqueous extract, 1 g of the powder was added to 100 mL of water and boiled at 80 °C for 30 min. The obtained decoction was separated by filtration, and a freshly prepared extract was used in the synthesis of the ZnS nanoparticles. After extraction, the solid biomass was stored separately for activation with acid.

Synthesis of ZnS nanoparticles

A zinc nitrate solution of 0.1 M was prepared, and to 50 mL of the solution, 50 mL of freshly prepared seed extract was added upon stirring. The addition of seed extract turned the solution yellowish, and stirring was continued while adding 50 mL of 0.1 M sodium sulfide solution drop by drop. Upon addition of sodium sulphide (Na_2S) drop by drop, a yellowish white precipitate formation was noticed, confirming the formation of

Fig. 1 Schematic of the synthesis of ZnS nanoparticles using *Manilkara zapota* seed extract, preparation of ZnS-loaded acid-activated biomass (ZnS-AAB), adsorption of humic acid, and subsequent conversion into nutrient-loaded alginate beads for controlled release applications.

ZnS, and after addition of all the Na_2S solutions, the stirring was continued further for 30 min at room temperature. The obtained product was later separated by centrifugation, and the solid product was washed with water and ethanol to remove impurities. Later, the yellowish white ZnS nanoparticles were dried in an oven at 80 °C for 120 min and stored in air tight containers for further characterization and use (Fig. 1).

Acid activation of biomass (AAB)

10 g of *M. zapota* seeds was used for aqueous extract preparation; the remaining biomass was dried in an oven at 80 °C for 60 min to remove moisture. To 5 g of dried biomass, 5 g of orthophosphoric acid was added and stirred to obtain a slurry mass. The slurry mass was placed in an oven and heated at 120 °C for 60 min to activate the biomass and make it carbon rich. After heating, the product was cooled to room temperature and later washed several times with water to neutralize the pH of the biomass and remove the leached organic matter. Once again, the water-washed biomass was dried in an oven at 80 °C for 120 min, and the dried activated biomass was characterized and used further (Fig. 1).

ZnS loading onto acid-activated biomass

In order to load ZnS nanoparticles onto acid-activated *M. Zapota* seed biomass, first, 1 g of ZnS nanoparticles was added to 50 mL of water and sonicated for 10 min to obtain a homogenous suspension. Similarly, 1 g of activated biomass was added to 50 mL of water and sonicated to obtain a dispersed suspension. Later, the suspension of the ZnS nanoparticles was added drop by drop to the biomass suspension under constant stirring on a magnetic stirrer. Stirring was continued for 60 min in order to allow the ZnS nanoparticles to load onto the activated biomass. The final ZnS-loaded acid-activated biomass was obtained by filtration and heated at 150 °C for 60 min to remove moisture and cure the product (Fig. 1). The dried product was named ZnS-loaded acid-activated biomass (ZnS-AAB). The ZnS loading onto the biomass was quantified using thermogravimetric analysis (Fig. S1). Based on the difference in residual mass between the pristine biomass and ZnS-loaded biomass, the ZnS loading was calculated to be approximately 1.9 wt%.

HA-adsorbed ZnS-AAB beads

To prepare the alginate beads, ZnS-AAB loaded with HA after the adsorption experiments was considered. Exactly, 1 g of HA-loaded ZnS-AAB collected from the adsorption experiments was added to 100 mL of 2% sodium alginate solution and stirred using a magnetic stirrer. To the same mixture while stirring, 20 mL of 1% KNO_3 solution was added, and stirring was continued for 30 min. A solution of 2% of 200 mL of calcium chloride solution was prepared, and to this solution, the alginate solution containing HA-loaded ZnS-AAB and KNO_3 was added drop by drop using a dropper. Upon the addition of the mixture to the calcium solution, beads were formed due to the crosslinking of calcium ions. The process was performed under sonication to obtain even spherical beads. After all components were added to the beaker, it was removed from the sonicator and set aside for 10 minutes to cure. The mixture was then filtered to obtain the beads. The obtained beads were washed with water to remove unreacted calcium and chloride ions from the surface and dried in an oven at 80 °C for 6 h. The oven-dried beads were characterized and used for further investigations.

Characterization

The ZnS nanoparticles, ZnS-AAB and ZnS-AAB beads were characterized using various analytical techniques to understand their formation and properties. The optical properties of the ZnS nanoparticles were measured using a UV-vis spectrophotometer (SHIMADZU, UV 3600 Plus) from 200 to 800 nm, and the humic acid concentration was recorded at a wavelength of 254 nm. The functional groups present on the ZnS, AAB, ZnS-AAB and ZnS-AAB beads were analyzed from 4000 to 400 cm^{-1} using an FTIR spectrophotometer (SHIMADZU, IRTRACER 100). The diffraction patterns of ZnS, composites and beads were recorded for 2θ values from 5 to 80 using powder X-ray diffraction (Bruker, D8). The surface morphology of the biomass and beads was visualized using HR-Scanning electron microscopy (Thermo Fisher Scientific), and the elemental profiles of the samples were obtained from EDX coupled with SEM. The size and shape of the ZnS nanoparticles were visualized with HR-transmission electron microscopy (Jeol-Japan).

Batch adsorption studies

The adsorption of HA by ZnS-AAB was performed in a batch adsorption process by optimizing the independent variables using RSM. All the experiments were performed using 50 mL of test solutions in a 100 mL conical flask using a mechanical shaker. The test solutions with ZnS-AAB were agitated at 100 rpm in a mechanical shaker, and ZnS-AAB was separated from the test solution by centrifugation at 5000 rpm. The supernatant solution was subjected to UV-visible light, and the absorbance was tested at 254 nm to calculate the residual concentration of HA in the resulting solution. The removal percentage and loading capacity of the ZnS-AAB were calculated using the following equations (eqn (1) and (2)):

$$\%\ \text{HA adsorption} = \frac{C_0 - C_1}{C_0} \times 100, \quad (1)$$

$$\text{Adsorption capacity} = \frac{C_0 - C_1}{m} \times V. \quad (2)$$

Box–Behnken design

Box–Behnken design (BBD) of response surface methodology (RSM) was adopted to optimize the independent variables, such as pH, contact time and initial concentration; further, they are economical due to fewer runs. Each independent variable was tested at three levels, as shown in Table 1. A total of 17 experimental runs were performed in this study based on the developed design matrix.

Table 1 Independent variables and their levels selected for the optimization of HA adsorption by ZnS-AAB

Factor	Name	Level	Low level	High level	Coding
A	pH	5.00	3.00	7.00	Actual
B	Contact time	75.00	30.00	120.00	Actual
C	Initial concentration	175.00	50.00	300.00	Actual

Water absorption behaviour

The water immersion method was adopted to study the water swelling index of the ZnS-AAB beads. To perform this study, 0.5 g of dry beads was immersed in 20 mL of water at room temperature (30 °C) and incubated with gentle manual stirring at regular time intervals. Every hour, the beads were removed from the water, wiped with tissue paper to remove the surface water and weighed. The swelling experiments were performed in triplicate, and the mean values were reported. The equilibrium water retention capacity was determined using the following equation (eqn (3)):

$$\mathrm{SI} = \frac{W_t - W_d}{W_d}, \quad (3)$$

where W_t is the weight of the beads at various time intervals and W_d is the weight of the dry beads.

Release of nutrients from alginate beads. The release of nutrients from the alginate beads was investigated by placing 0.1 g of beads in 100 mL of 0.1% calcium solution. A calcium solution was used in this study to create a hard water environment. Every day, 5 mL of the solution was drawn, and an equal volume of calcium solution was added to the test solution for 2 weeks. The collected samples were subjected to UV and flame photometry to determine the concentrations of K^+, NO_3^- and HA nutrients.

Results and discussion

Characterization

UV-vis spectroscopy. ZnS nanoparticles are well known for their optical properties due to which they have wide applications in various domains. In this study, the ZnS nanoparticles synthesized using the aqueous extract of *Manilkara zapota* seeds were subjected to UV-visible analysis, and the results are presented in Fig. 2. The plot exhibits a decreasing trend from 200 nm and is found to have a hump at approximately 325 nm, which confirms the first electron transition 1Se–1Sh due to the quantum confinement of charge carriers, resulting in a smaller particle size of ZnS.[13] Further, the band gap of the ZnS nanoparticles was calculated using the Tauc plot and found to be 3.16 eV, which was lower than that of the bulk ZnS (~3.7 eV).[14] Although nanoscale ZnS typically shows band gap widening due to quantum confinement, the observed reduction indicates that surface effects dominate in the present system. At particle sizes below 2 nm, a high surface-to-volume ratio promotes the formation of defect states (*e.g.*, sulfur vacancies), while phytochemical capping further modifies the surface electronic structure, which is in good agreement with the literature.[15–17]

FTIR spectroscopy. The FTIR spectra of ZnS nanoparticles, acid-activated biomass, ZnS-loaded biomass, humic acid-loaded ZnS-biomass and humic acid-loaded ZnS-biomass beads are depicted in Fig. 3. The FTIR spectra of ZnS nanoparticles displayed several peaks corresponding to various

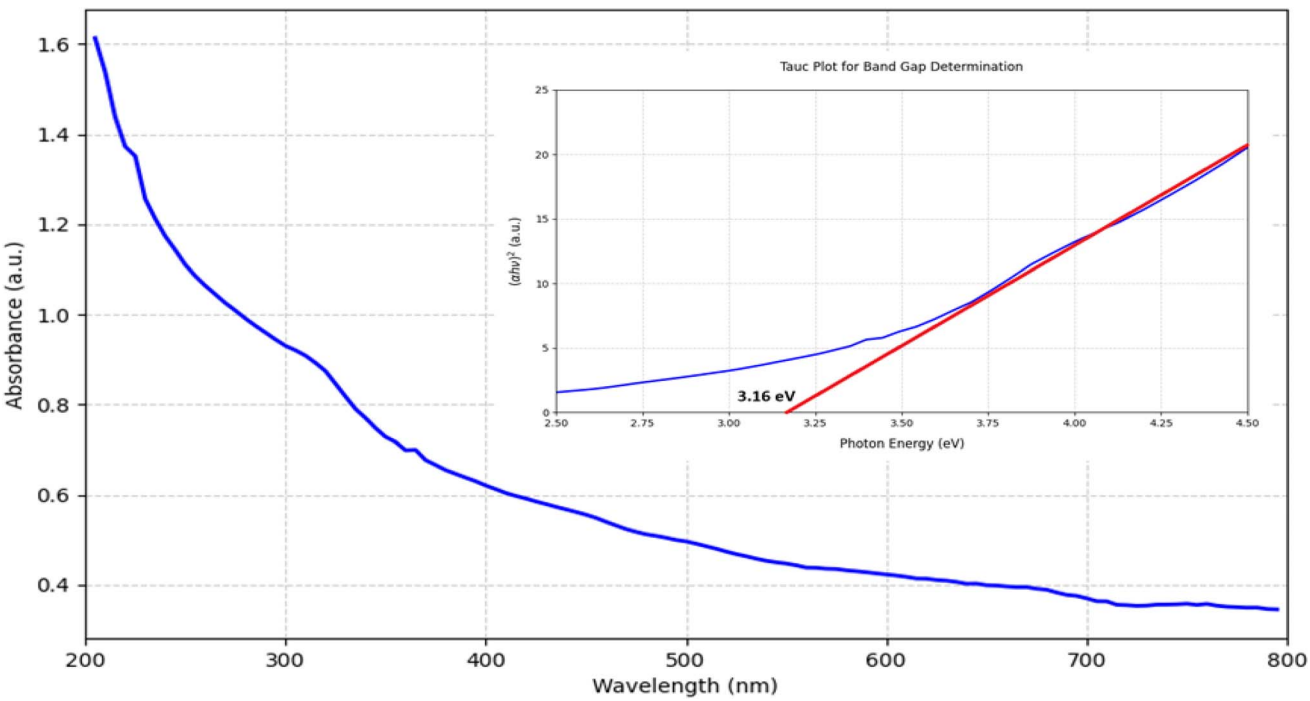

Fig. 2 UV-vis spectra of ZnS nanoparticles synthesized using the aqueous extract of *Manilkara zapota* seeds.

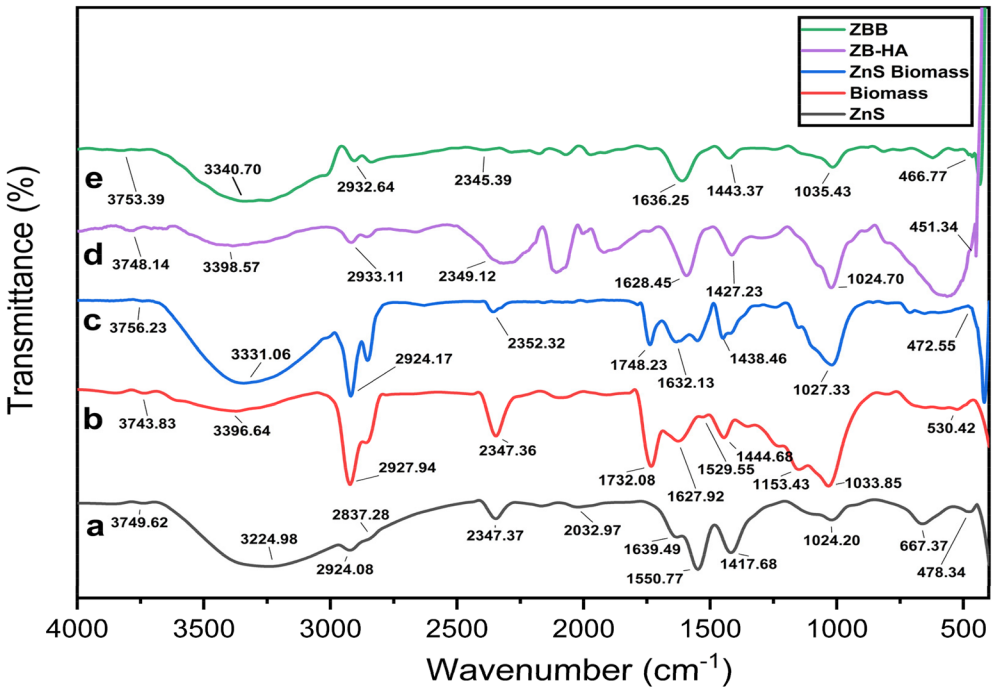

Fig. 3 FTIR spectra of (a) ZnS nanoparticles synthesized using the aqueous extract of *Manilkara zapota* seeds, (b) acid-activated *Manilkara zapota* seed biomass, (c) ZnS nanoparticle-loaded acid-activated *Manilkara zapota* seed biomass, (d) HA-ZnS-AAB (e) HA-ZnS-AAB alginate beads.

functional groups that assisted in the synthesis and stabilization of nanoscale ZnS (Fig. 3a). A broad peak at 3224 cm^{-1} corresponds to the hydroxyl group stretching vibrations of biomolecules, such as flavonoids and phenols, in the aqueous extract of *Manilkara zapota* seeds. Sharp peaks at 2924 and 2837 cm^{-1} represent methyl group stretching vibrations. A peak at 1639 cm^{-1} is due to bending vibrations of hydroxyl groups, and this could be due to the presence of moisture in the ZnS nanoparticles. The asymmetric and symmetric stretching vibrations of carboxylate groups were observed at 1550 and 1417 cm^{-1}, respectively, and the C–O stretching of alcohols was observed at 1024 cm^{-1}. In general, all metal-oxide and metal-sulphide bond peaks are usually observed between 450 and 670 cm^{-1}.[18] In this study, a less intense peak at 478 cm^{-1} was observed, which could be attributed to the Zn–S stretching vibration. The presence of biomolecules on the surface of the ZnS nanoparticles can interact with the biomass surface by π–π interactions and assist in surface binding. Further, the biomolecules can electrostatically attract HA towards the surface of the ZnS nanoparticles and synergistically enhance the HA adsorption. The FTIR of acid-activated biomass from *Manilkara zapota* seeds exhibited a number of peaks, indicating a variety of functional groups (Fig. 3b). A small peak at 3743 cm^{-1} indicates a free hydroxyl group that arises due to the heating and acid treatment of the biomass. A strong intense peak at 2927 cm^{-1} indicates methyl group dominance due to pretreatment with acid. A peak at 1732 cm^{-1} represents the carbonyl ketone group molecules of biomass. A medium-intense band at 1627 cm^{-1} is due to carboxylate group asymmetric stretching vibrations, and the functional group presence is supported by the symmetric stretching vibrations observed at 1529 cm^{-1}. The aromatic C–H asymmetric vibrations are noticed with a peak at 1444 cm^{-1}, and peaks at 1153 and 1033 are due to the C–O stretching of polysaccharides. The characteristic peaks of biomass and ZnS around 470 cm^{-1} was observed in ZnS-loaded biomass, confirming the successful loading of ZnS onto the surface of biomass (Fig. 3c). Similarly, the humic acid-loaded ZnS-biomass also resulted in very identical bands with additional bands in the fingerprint region below 800 cm^{-1}, which is due to humic acid with shifted Zn–S peak at 451 cm^{-1}, and the shift is due to binding of humic acid onto the surface of the ZnS nanoparticles (Fig. 3d). The beads of humic acid-loaded ZnS nanoparticle biomass exhibited the characteristic peaks of ZnS and biomass (Fig. 3e). The results of FTIR highlight the successful incorporation of humic acid-loaded ZnS biomass into beads.

XRD analysis. The powder X-ray diffraction of ZnS, biomass, ZnS-biomass, ZnS beads and ZnS-biomass beads are illustrated in Fig. 4. The XRD of ZnS nanoparticles synthesized using the aqueous extract of *Manilkara zapota* seeds yielded three distinct peaks at 2θ values of 28.5°, 47.5° and 56.3°, suggesting the formation of cubic phase, and the broad peaks indicate their smaller crystalline size (Fig. 4a). Since the synthesis of ZnS nanoparticles was performed at lower temperatures, the zinc blende phase dominates the formation. The patterns are in good agreement with JCPDS card no. 01-079-0043 and are additionally supported by literature reporting the green synthesis of ZnS nanoparticles.[19] The crystallite size of ZnS

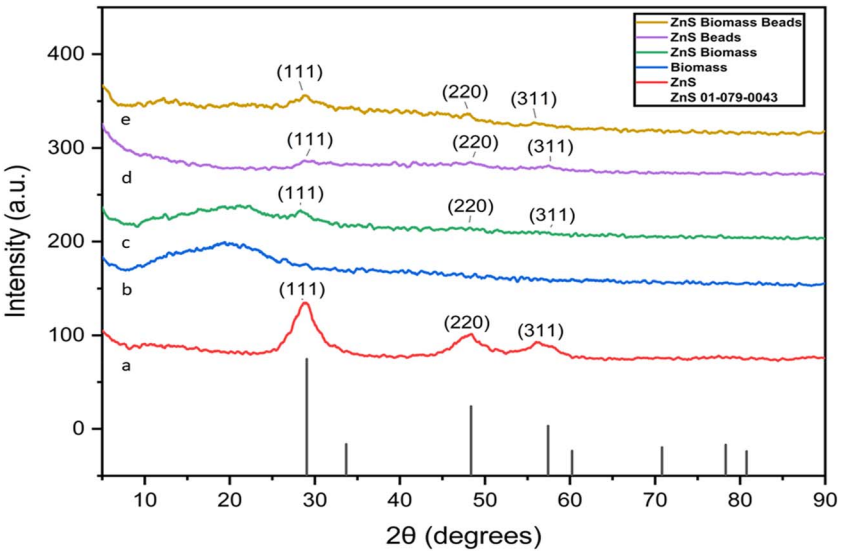

Fig. 4 XRD patterns of (a) ZnS nanoparticles, (b) biomass, (c) ZnS-loaded biomass, (d) ZnS nanoparticle beads and (e) HA-ZnS-AAB bead containing K^+ and NO_3^- ions.

nanoparticles was estimated using the Scherrer equation from XRD peak broadening and found to be ~2.44 nm. The XRD of the acid-activated *Manilkara zapota* seed biomass displayed a broad peak with a maximum at 19°, which is due to the semi-crystalline structure of cellulose, and the broad peak is a result of disordered regions of the cellulose (Fig. 4b). The characteristic peaks of the ZnS nanoparticles and biomass were evidenced in the ZnS-loaded biomass (Fig. 4c). However, the intensity of the ZnS peaks was low compared to pure ZnS, which is due to the low percentage of ZnS present on the surface of the biomass. The ZnS alginate beads exhibited characteristic peaks of ZnS nanoparticles; however, no other peaks were evidenced (Fig. 4d); similarly, the ZnS-loaded biomass beads containing HA, K^+ and NO_3^- exhibited weak characteristic ZnS peaks (Fig. 4e).

SEM analysis. The scanning electron microscopy technique was used to visualize the surface morphology of pristine biomass, AAB, ZnS-AAB, humic acid, and K^+ and NO_3^- ion-loaded ZnS-biomass alginate beads. The results are presented in Fig. 5. The pristine biomass surface was observed to be rough and layered (Fig. 5a). The surface of acid-activated biomass is found to be porous and uneven, as shown in Fig. 5b. Acid activation resulted in the development of porosity on the surface of the biomass, making it ideal for adsorption investigations.[20] The surface of the ZnS-loaded biomass also exhibited a similar surface with porosity; however, an even distribution of ZnS nanoparticles on its surface is clearly evidenced, confirming the loading of ZnS nanoparticles onto the surface of the acid-activated biomass (Fig. 5c). The composite bead reveals a spherical shape and uneven surface with no cracks on its surface (Fig. 5d).

EDX analysis. The elemental analysis obtained from SEM investigations provided valuable information on the elements present, and EDX patterns obtained in this study are summarized in Fig. 6. The elemental profile of acid-activated biomass showed elemental peaks of C, O, P and S (Fig. 6a). The elements C, O and S are due to the biomass molecules containing C, O and S compounds, and the P peak is due to acid activation of biomass with ortho phosphoric acid. The elemental profile of ZnS-loaded biomass reveals the presence of Zn and S elements in addition to C, O, S and P, which are present in biomass (Fig. 6b). The presence of additional characteristic peaks confirms the loading of ZnS nanoparticles onto the surface of the acid-activated biomass. For a better understanding on the distribution of ZnS nanoparticles onto the surface of the AAB, EDX mapping was performed (Fig. 6d and e). The EDX mapping shows the even distribution of ZnS nanoparticles onto the surface of AAB. The elemental profile of the beads highlighted the successful preparation of ZnS-biomass beads with K^+ ions. The Ca element peak is from calcium cross-linked beads of alginate, and K is due to the addition of KNO_3 at the time of preparation of the beads (Fig. 6c). An additional intense chloride peak is noticed, which is due to $CaCl_2$ solutions used in the preparation of the beads. The absence of nitrogen in the EDX spectrum is attributed to the inherent limitations of EDX analysis in detecting elements with low atomic numbers. Nitrogen, being a light element, often exhibits weak signals that fall below the detection limit of the instrument and overlap with the signals of carbon and oxygen.

TEM analysis. A transmission electron microscope was used to visualize the size and shape of the ZnS nanoparticles synthesized using aqueous extracts of *Manilkara zapota* seeds. The images revealed the formation of ZnS nanoclusters with a size less than 2 nm and irregular shapes (Fig. 7). Initially, at 20 nm scale magnifications (Fig. 7a), the shape seems to be spherical with agglomerations, but at a scale of 2 nm (Fig. 7b), the shapes of the ZnS are found to be irregular with no specific shapes. Though the particles are agglomerated, the total agglomerated particle sizes are in the nanoscale range. This agglomeration is due to the biomolecules of the aqueous

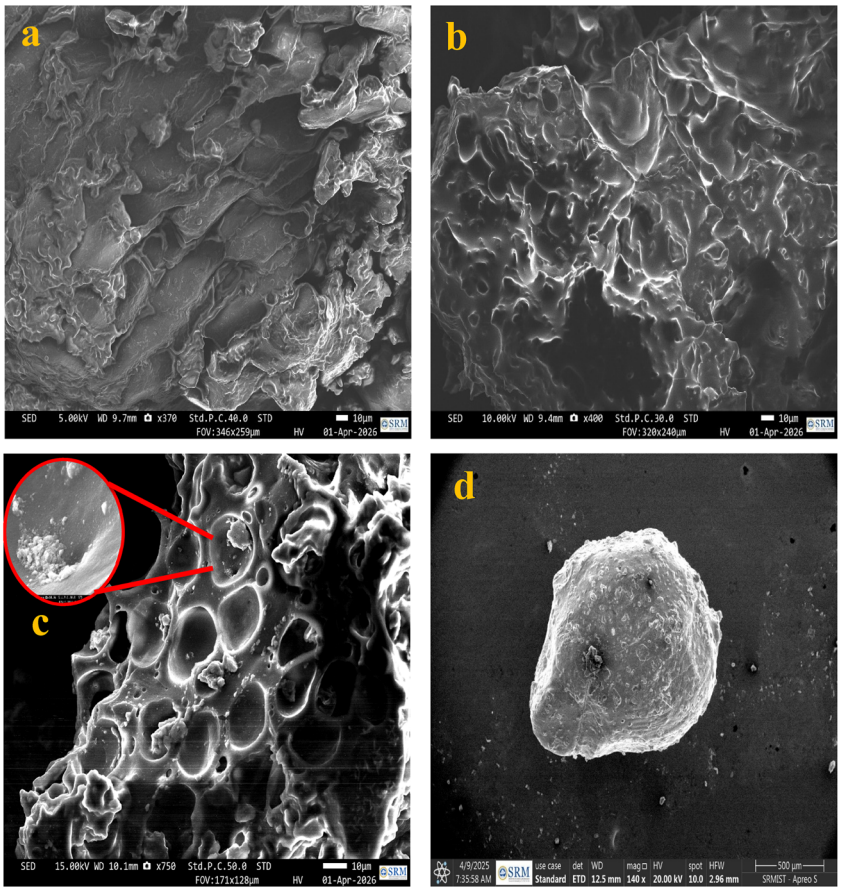

Fig. 5 SEM images of (a) pristine biomass, (b) acid-activated biomass, (c) ZnS-loaded acid-activated biomass and (d) ZnS-biomass bead containing humic acid and K^+ and NO_3^- ions.

extracts of *Manilkara zapota* seeds binding to each other due to intermolecular hydrogen bonding.[21] A particle size distribution histogram (Fig. 7c) was constructed from TEM images by measuring multiple particles, which yielded an average particle size of ~1.39 nm. This is in close agreement with crystallite size (~2.44) nm calculated from XRD for ZnS nanoparticles. The TEM-EDX (Fig. 7d) confirms the elemental composition of the green synthesized ZnS nanoparticles. The EDX spectrum clearly shows the presence of Zn and S as the major constituents, which confirms the successful formation of ZnS nanoparticles. Quantitative analysis reveals that Zn and S are present with weight percentages of 68.55% and 31.45%, respectively. The absence of extra impurity peaks indicates that the green-synthesized ZnS nanoparticles are highly pure. Small signals related to carbon (C) and copper (Cu) are also observed. These are likely caused by the carbon-coated copper grid used in the TEM analysis; additionally, the C peak is due to the biomolecules capped onto the surface of the ZnS nanoparticles. Overall, the EDX results confirm the elemental makeup and successful formation of the ZnS nanoparticles.

BBD of HA adsorption. The optimization of independent variables such as pH, contact time and initial concentration towards HA removal by ZnS-AAB was performed using BBD, and the results of the experimental design in terms of % removal are summarized in Table 2. It is noticed that the % removal obtained *via* experimental runs is in good agreement with the predicted values, highlighting the suitability of the developed design. The alignment of experimental values and predicted values along a straight line further confirms the suitability of the design, and the Box–Cox lambda value is found to be close to 1, suggesting no transformation requirements for the developed design (Fig. 8). The ANOVA of the experimental values obtained in this study for the removal of HA by ZnS-AAB is summarized in Table 3. The applicability of the significance of the present design is determined from the *F*-value and *p*-value, and in this study, an F-value of 408.25 with a *p*-value <0.0001 highlights the reliability of the model. The performance of the model is further assessed by the standard deviation, mean, CV% and R^2 values. In this study, a standard deviation of 1.15 with a mean of 64.34 provides the strong predictive accuracy of the present model, and the high precision of the model is evidenced by the CV (1.78%). Adding to the accuracy and precision of the model, the R^2 values further support the observations, and the experimental, adjusted and predicted R^2 values are all close to 1. An adequate precision value indicates an excellent predictive capability of the model and readiness to navigate for optimization.[22] A value of 69.27 in this study provided an

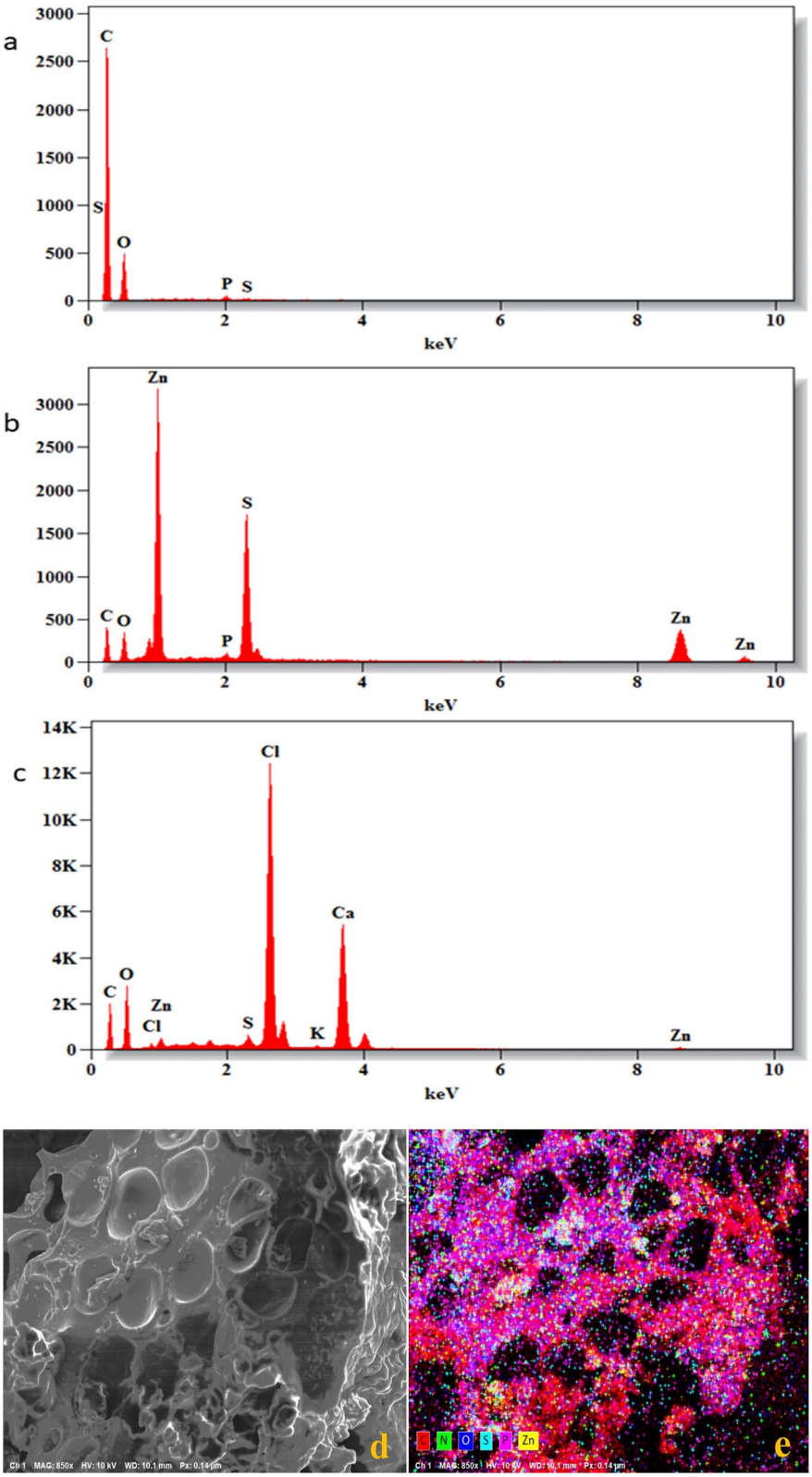

Fig. 6 EDX profile of (a) acid-activated biomass, (b) ZnS-loaded acid-activated biomass and (c) ZnS-biomass bead containing humic acid and K^+ and NO_3^- ions. (d) SEM image of ZnS-AAB used for elemental mapping and (e) ZnS-AAB elemental mapping.

outstanding signal-to-noise ratio with excellent predictive capability and indicated the robustness of the model. All these results confirm the exceptional reliability of the optimization process for the removal of HA by ZnS-AAB. The experimental quadratic equation for the removal of HA by ZnS-AAB is provided as follows (eqn (4)):

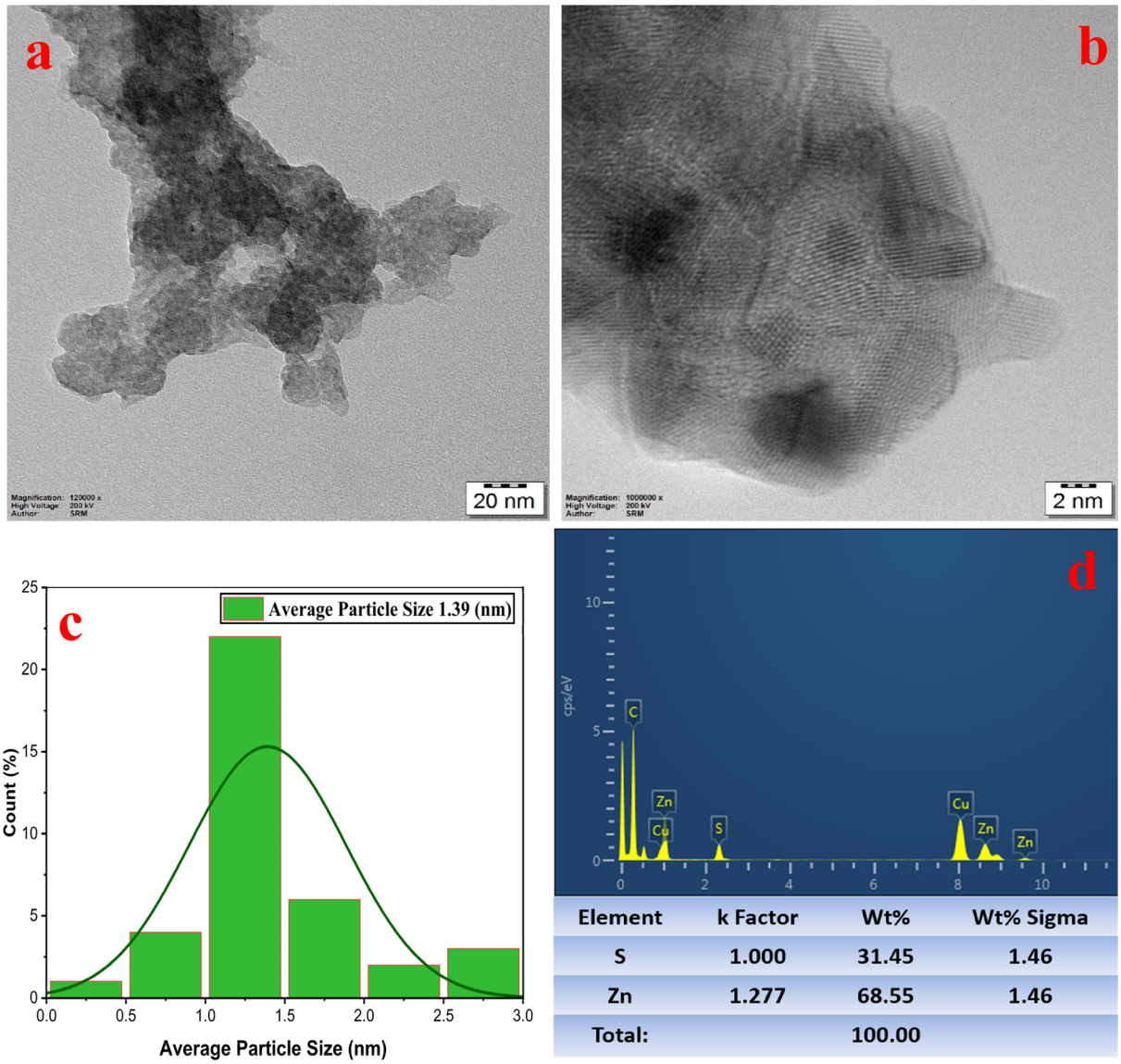

Element	k Factor	Wt%	Wt% Sigma
S	1.000	31.45	1.46
Zn	1.277	68.55	1.46
Total:		100.00	

Fig. 7 TEM images of ZnS nanoparticles in (a) 20 nm scale magnification and (b) 2 nm scale magnification. (c) TEM-histogram for average particle size distribution and (d) TEM-EDX for ZnS nanoparticles synthesized using the aqueous extracts of *Manilkara zapota* seeds.

$$\text{Removal} = 80.62 - 7.01A + 9.91B - 12.40C + 0.42AB - 5.15AC - 1.45BC - 20.07A^2 - 7.42B^2 - 7.10C^2. \quad (4)$$

The 3D surface plots of independent variable interaction provide valuable information on the optimization of independent variables,[23] and the plots obtained in this study are presented in Fig. 9. The 3D plot of pH *vs.* contact time (Fig. 9a) indicates that the maximum removal efficiency is noted at pH 4 and later decreases with an increase in pH. At pH 4, HA remains protonated, and this allows HA to form hydrogen bonding, hydrophobic interactions and van der Waals forces, making it ideal for maximum adsorption. Further, the compact size of HA at low pH further makes it accessible to the surface sites for binding. When the pH increases, the surface functional groups of HA deprotonate and attain a negative charge, which may repel due to the same charges and further increase the size of the HA molecule.[10] The pH_{pzc} of ZnS-AAB was experimentally determined to be at pH 5.1 (Fig. S3), and this makes it favorable for the adsorption of HA at pH 4. At pH 4, the concentration of HA was found to increase with an increase in contact time, and this is due to the fact that at higher contact times, HA has enough time to interact with the surface sites for enhanced adsorption. In the case of pH *vs.* initial concentration (Fig. 9b), maximum removal was evidenced at pH 4. However, with a rise in the initial concentration, the removal efficiency decreased, and this is due to the exhaustion of surface-active sites for the binding of HA.[24] Similarly, in the case of contact time *vs.* initial concentration (Fig. 9c), the removal efficiency remained high at higher contact times with lower concentrations. With an increase in initial concentrations, the efficiency was found to be low despite increasing the contact time. A cube plot is

Table 2 BBD runs with experimental and predicted values

Std	Run	A: pH	B: contact time (min)	C: initial concentration (mg L^{-1})	Removal%	
					Exp	Predicted
15	1	5	75	175	80.5	80.62
6	2	7	75	50	62.9	63.99
8	3	7	75	300	28.1	28.89
11	4	5	30	300	44.6	45.24
12	5	5	120	300	62.5	62.16
7	6	3	75	300	54.3	53.21
5	7	3	75	50	68.5	67.71
14	8	5	75	175	80.6	80.62
16	9	5	75	175	80.9	80.62
17	10	5	75	175	80.5	80.62
13	11	5	75	175	80.6	80.62
2	12	7	30	175	37.2	35.78
4	13	7	120	175	56.9	56.45
10	14	5	120	50	90.5	89.86
3	15	3	120	175	68.2	69.63
1	16	3	30	175	50.2	50.65
9	17	5	30	50	66.8	67.14

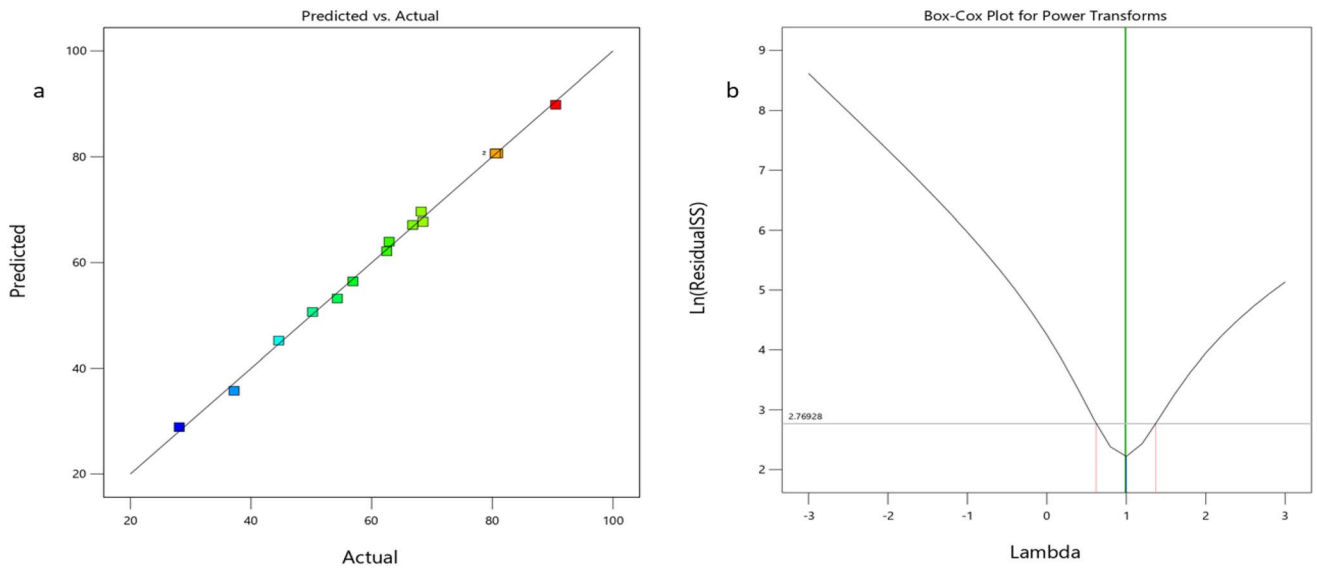

Fig. 8 (a) Predicted *vs.* actual value distribution plot and (b) Box–Cox plot for transforms obtained for the removal of HA by ZnS-AAB.

a powerful decision-making tool for identifying optimal conditions, and a cube plot of the interaction of the three independent variables obtained in this study is shown in Fig. 9d. The plot indicates the optimal conditions for the maximum removal of HA by ZnS-AAB, and the pH is found to be the most critical factor of influence, followed by contact time. The optimal conditions for this study are pH < 5, contact time > 120 min and moderate initial concentrations.

Adsorption isotherms. To understand the type and process of the adsorption of HA by ZnS-AAB, adsorption isotherms such as Langmuir, Freundlich, D–R and Temkin isotherm models were used to analyze the equilibrium data. The non-linear plots of isotherm models are presented in Fig. 10, and their respective constants and coefficients are summarized in Table 4. The correlation coefficients of all the models are close to one, suggesting their applicability, with the Langmuir isotherm being very close to one.[25] It is also important to consider the other constants of the models to understand the adsorption process. The Freundlich constants K_f and n were noted to be 85.32 and 3.45, respectively, and any value of $n > 1$ makes the adsorption favorable. The q_m value calculated from the Langmuir isotherm was found to be 297.5 mg g^{-1}, and this is in good agreement with the experimental q_m value of 293.7 mg g^{-1}. The K_L value of 0.023 indicates the stronger affinity of HA towards ZnS-AAB for adsorption. Further, the K_L value obtained in this study was used to determine the dimensionless separation factor (R_L), and it was noticed that for all the studied concentrations of HA (50–300 mg L^{-1}), the R_L values were found to be between 0.12 and

Table 3 ANOVA of HA removal by ZnS-AAB

Source	Sum of squares	df	Mean square	*F*-value	*p*-value
Model	4839.82	9	537.76	408.25	<0.0001
A-pH	393.40	1	393.40	298.66	<0.0001
B-contact time	786.06	1	786.06	596.76	<0.0001
C-initial concentration	1230.08	1	1230.08	933.85	<0.0001
AB	0.7225	1	0.7225	0.5485	0.4830
AC	106.09	1	106.09	80.54	<0.0001
BC	8.41	1	8.41	6.38	0.0394
A^2	1696.44	1	1696.44	1287.90	<0.0001
B^2	231.97	1	231.97	176.11	<0.0001
C^2	212.10	1	212.10	161.02	<0.0001
Residual	9.22	7	1.32		
Lack of fit	9.11	3	3.04		
Pure error	0.1080	4	0.0270		
Cor total	4849.04	16	R^2	0.998	
Std. dev	1.15		Adjusted R^2	0.995	
Mean	64.34		Predicted R^2	0.969	
CV%	1.78		Adequate precision	69.27	

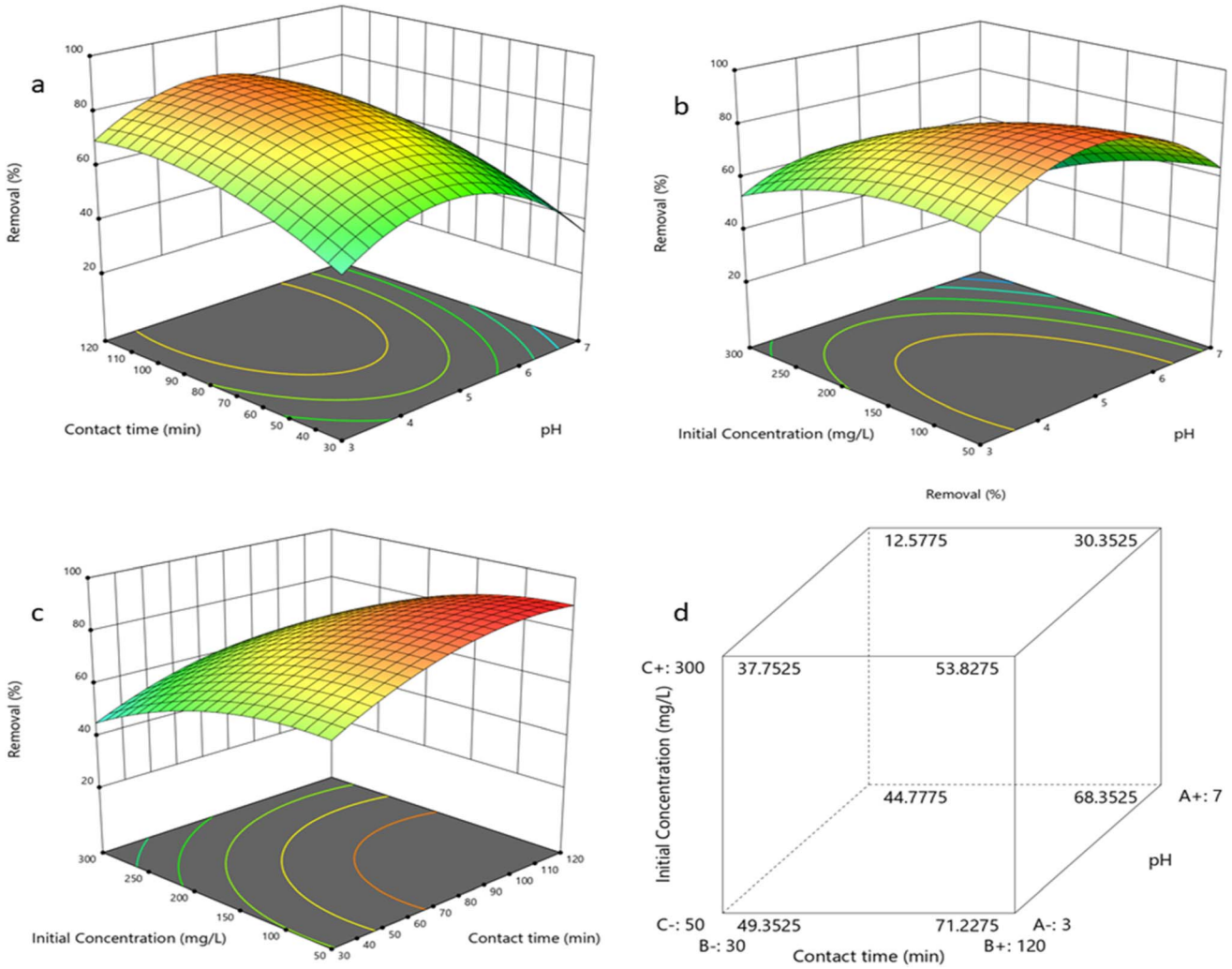

Fig. 9 3D surface plots of (a) pH *vs.* contact time, (b) pH *vs.* initial concentration, (c) contact time *vs.* initial concentration and (d) cube plot for % removal with independent variables for the removal of HA by ZnS-AAB.

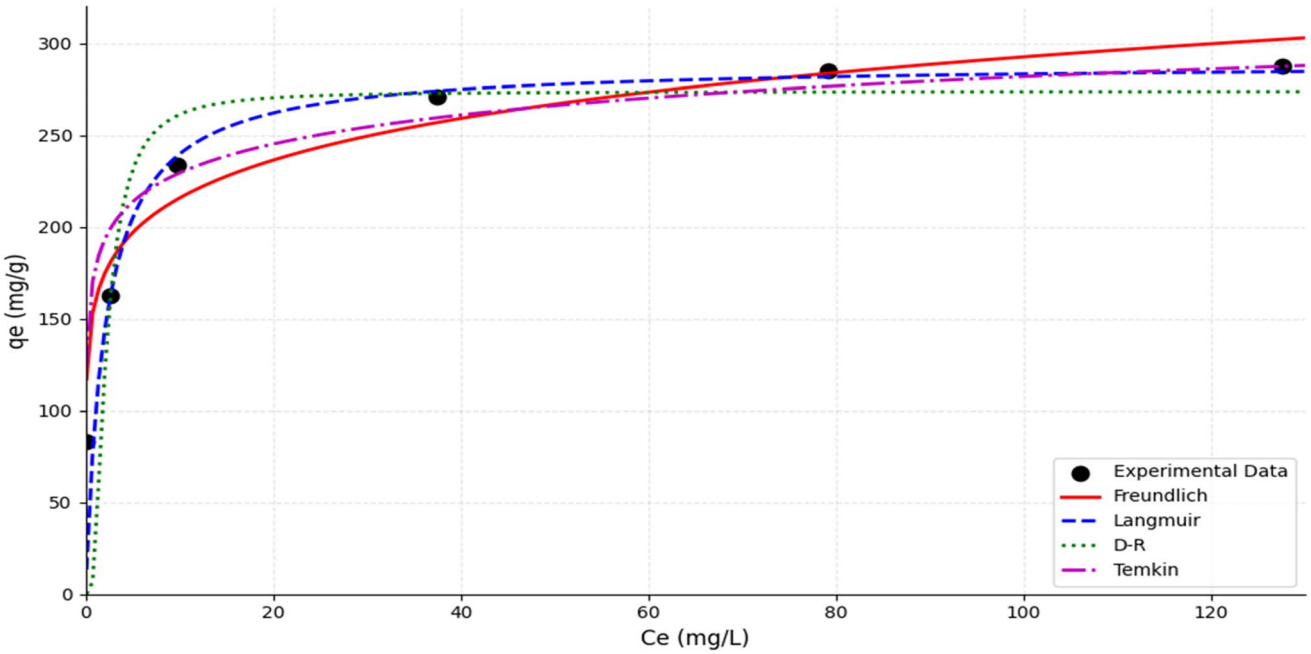

Fig. 10 Non-linear isotherm plots obtained for the removal of HA by ZnS-AAB under equilibrium conditions (pH 4 and contact time 120 min).

Table 4 Constants and coefficients of isotherm models obtained for the removal of HA by ZnS-AAB

Isotherm	Equation	Constants	Values	RMSE (mg g^{-1})	AARE (%)
Freundlich	$q_e = K_F C_e^{\frac{1}{n}}$	K_f (mg g^{-1})	85.32	12.45	6.23
		N	3.45		
		R^2	0.982		
Langmuir	$q_e = \frac{Q_m K_L C_e}{1 + K_L C_e}$	q_m (mg g^{-1})	297.5	4.87	2.15
		K_L (L mg^{-1})	0.023		
		R^2	0.999		
D–R	$q_e = q_s \exp\left(-K_{DR}\left[RT \ln\left(1 + \frac{1}{C_e}\right)\right]^2\right)$	Q_m (mg g^{-1})	275.1	15.62	7.84
		K_{D-R}	3.22×10^{-7}		
		E (kJ mol^{-1})	12.45		
		R^2	0.974		
Temkin	$q_e = \frac{RT}{b_T} \ln(A_T C_e)$	A (L mg^{-1})	0.045	18.76	9.45
		B (mg g^{-1})	62.34		
		R^2	0.953		

0.46, suggesting that the HA adsorption by ZnS-AAB is favorable under all conditions (Table S1). The Q_m value obtained from the D–R isotherm was determined to be 275.1 mg g^{-1}, which is quite close to the experimental value; the mean free energy of the adsorption is found to be 12.45 kJ mol^{-1}, and it indicates that the mechanism is ion-exchange; however, it also falls within the range of physical adsorption.[22] A low value of A (0.045) and a high value of B (62.34) obtained for Temkin constants indicate lower repulsion and higher physical adsorption possibilities for the removal of HA by ZnS-AAB.

Correlation coefficients are one important indicator of the better applicability of isotherm models to equilibrium data, and researchers use them in decision making. However, in this study, the correlation coefficients for the four isotherm models are close to one. Since the correlation coefficients are close to one, it is imperative to decide which is the best fitting model to the data, and error analysis was performed to identify the best-suited model. The error analysis revealed that the Langmuir isotherm has the lowest RMSE and AARE compared to the other three isotherm models, making it the most suitable model for the removal of HA by ZnS-AAB, and Temkin is the least suitable model (Table 4). Thus, the better fit of the Langmuir model highlights the monolayer adsorption dominance over multi-layer adsorption.

Kinetics of adsorption. The kinetic data obtained at various temperatures were subjected to four kinetic models in order to understand the rate of reaction of the binding mechanism, and the results are summarized in Table 5 and Fig. 11 for 303 K and in Tables S2–S3 and Fig. S4 for 313 and 323 K. It is interesting to see that the selected kinetic models exhibit a good fit to the

Table 5 Kinetic constants obtained for the removal of HA by ZnS-AAB at 303 K (initial concentration 50 mg L^{-1})

Model	Constants	Value	RMSE	AARE (%)
Pseudo first order	q_e (mg g^{-1})	83.5	3.21	4.12
	k_1 (min^{-1})	0.045		
	R^2	0.985		
Pseudo second order	q_e (mg g^{-1})	85.2	1.05	1.33
	k_2 (mg g^{-1} min^{-1})	0.0012		
	R^2	0.998		
Elovich	α (mg (g min)$^{-1}$)	2.45	2.34	2.89
	β (g mg^{-1})	0.087		
	R^2	0.992		
Intraparticle	k_{id} (mg (g $min^{0.5}$)$^{-1}$)	6.34	5.67	7.45
	C (mg g^{-1})	18.4		
	R^2	0.934		

kinetic data based on correlation coefficients being close to one. The q_e values of the first and second orders were close to the experimental values, suggesting the applicability of the models. However, the mechanism of binding of HA by ZnS-AAB can be determined only when the best kinetic model is identified, and in order to find the best fit model, error analysis was performed for the kinetic data at all temperatures. It was identified that pseudo second order has the least errors, with an RMSE of 1.05 and an AARE of 1.33. The RMSE and AARE of the other three models were higher compared to the pseudo second order model, suggesting the best fit of the model to the kinetic data of HA removal by ZnS-AAB. The Elovich model also exhibited higher correlation coefficients with the least errors next to that of the pseudo second order. The α values obtained from the Elovich model were found to decrease with an increase in temperature; this indicates that adsorption is favoured at lower temperatures, and this is supported by the decreasing loading capacities observed experimentally and by the pseudo first and second order models. The intraparticle diffusion plots suggested that pore diffusion is not the only process with multi linear plots.[26] The kinetic experiments were performed at higher temperatures, and it was observed that the rate of reactions of pseudo first- and second-order were found to increase; however, the loading capacities were found to decrease with an increase in temperature. The higher the temperature, the greater the impact on the loading capacity (Tables S2 & S3). The decrease in loading capacities is due to the weakening of adsorption sites and an increase in the disorderliness of HA. These observations suggest that higher temperatures make the adsorption of HA by ZnS-AAB unfavourable. Further, the kinetic data were analysed with the Arrhenius equation to determine the activation energy, which was found to be 24.5 kJ mol^{-1}. The activation energy suggests that physisorption is the mechanism of the binding of HA by ZnS-AAB, and this is in good agreement with the mean free energy value obtained from the Dubinin–Radushkevich isotherm (D–R isotherm).

Table 6 Thermodynamic data for the binding of HA by ZnS-AAB from aqueous solutions

Temperature (K)	$\Delta G°$ (kJ mol^{-1})	$\Delta H°$ (kJ mol^{-1})	$\Delta S°$ (kJ K mol^{-1})
303	−5.78	−15.72	−0.032
313	−5.45		
323	−5.12		

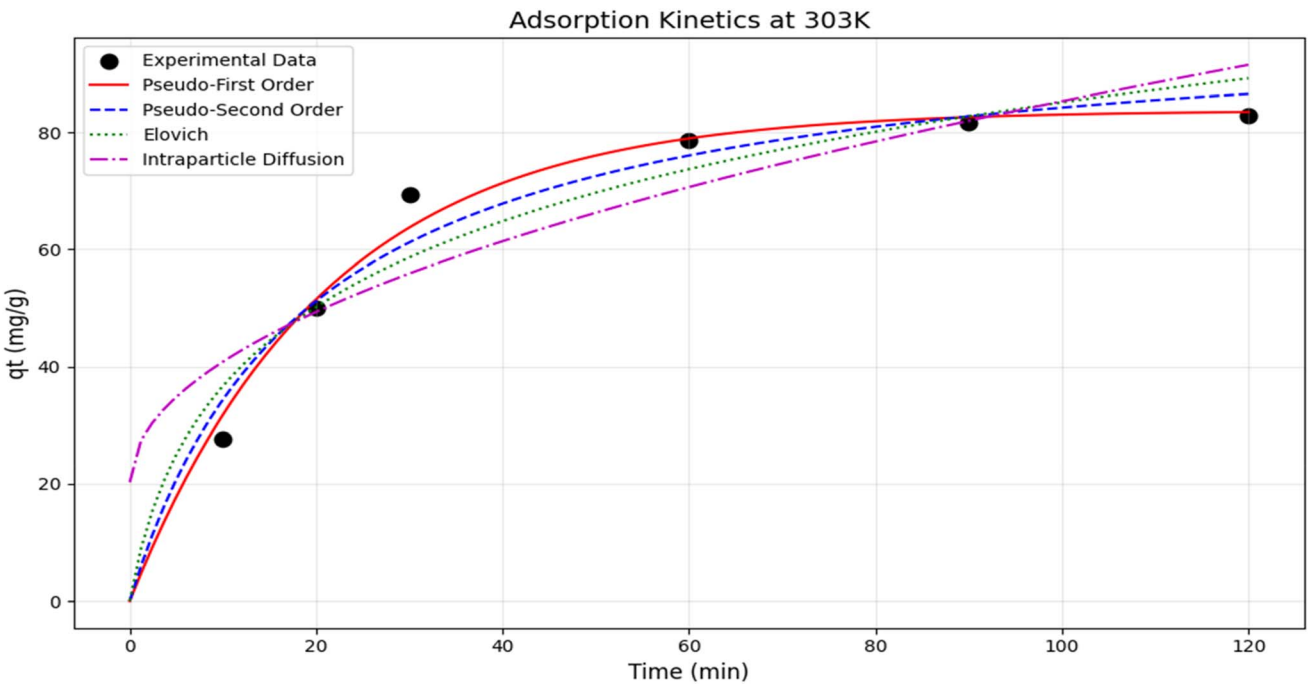

Fig. 11 Kinetic plots obtained for the removal of HA by ZnS-AAB at 303 K.

Thermodynamics of HA binding by ZnS-AAB. Thermodynamic investigations revealed crucial information on the binding of HA by ZnS-AAB onto their surface, and the results of the investigation are summarized in Table 6. The change in free energy (ΔG°) was found to be negative at all studied temperatures, suggesting the spontaneous nature of the adsorption of HA by ZnS-AAB. It is observed that with an increase in temperature, the spontaneity decreases, and this is in good agreement with the kinetic data obtained in this study at various temperatures. The negative enthalpy values suggest that the process is exothermic and that the heat release value of 15.72 kJ mol^{-1} falls in the range of physical adsorption, which is consistent with the observed activation energy value.[27] The negative entropy values suggest a decrease in randomness with the orderly arrangement of HA molecules onto the surface of the ZnS-AAB. Overall, the results conclude that adsorption is favourable and preferred at lower temperatures for the adsorption of HA by ZnS-AAB.

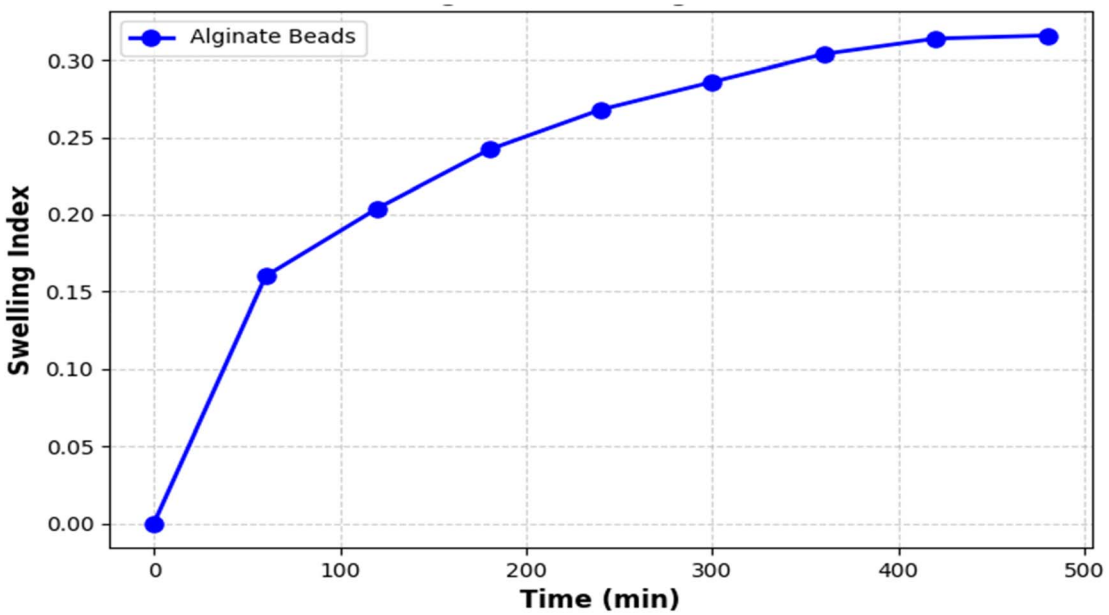

Fig. 12 Swelling index plot of HA-loaded ZnS-AAB alginate beads in water.

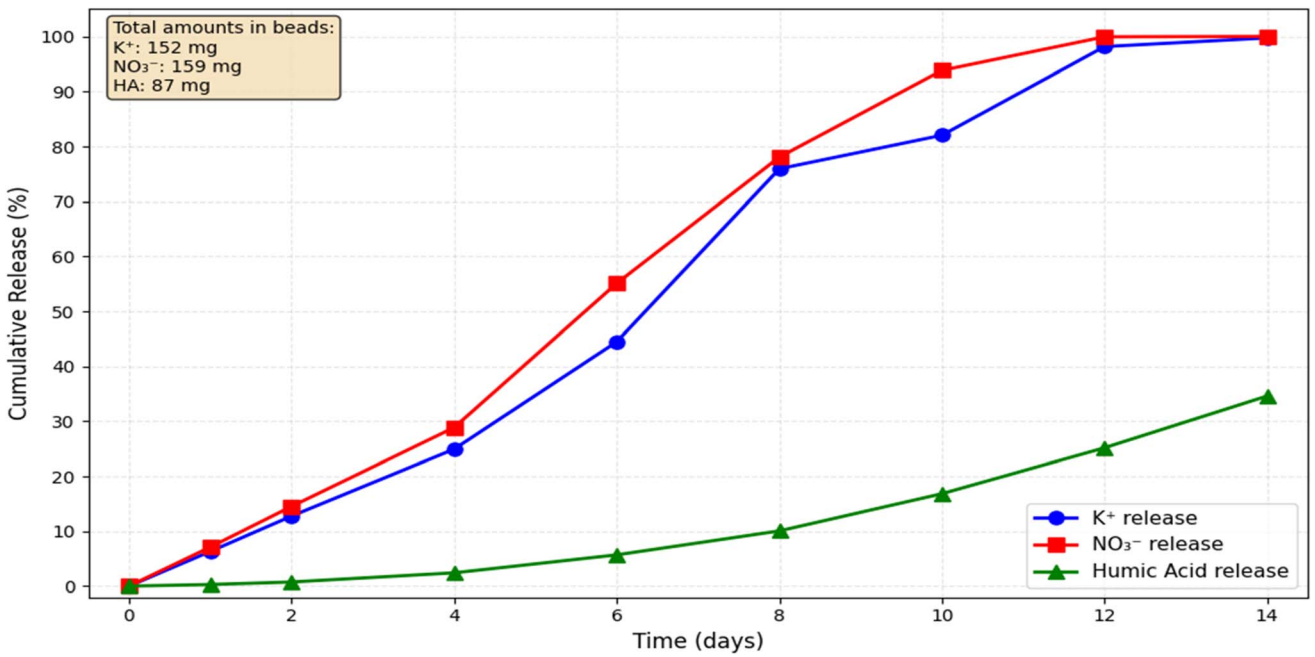

Fig. 13 Cumulative release of K^+ and NO_3^- ions and HA from alginate beads in a calcium solution.

Encapsulation of HA-loaded ZnS-AAB into alginate beads. Most studies aim at investigating the regeneration of the adsorbent for reuse in multiple cycles, but the adsorbate reuse has been ignored or unexplored. In this study, for the first time, the reuse of the adsorbate-loaded adsorbent is explored for use in agricultural applications, making the adsorption process sustainable with circular thinking. The HA-loaded ZnS-AAB was encapsulated into alginate beads with the addition of KNO_3 to make it prolific for agricultural applications. The alginate beads with biomass help in the retention of water and maintain soil moisture during drought or arid conditions, and added minerals and HA assist in plant growth and maintain soil fertility.[28,29] Further, the beads assist in the controlled release of the essential minerals that support plant growth without polluting the soil or surface runoff unlike fertilizers.[30] The successful encapsulation of HA-loaded ZnS-AAB into alginate beads was evidenced by EDX analysis, which indicated the essential nutrients required for plant growth, such as NPK.

Table 7 Kinetic data of nutrient release from HA-loaded ZnS-AAB alginate composite beads

Model	Nutrients	k	n	R^2	Adj R^2	RMSE
Zero-order	K^+	8.279	—	0.946	0.937	8.426
	NO_3^-	7.844	—	0.964	0.950	7.570
	HA	1.927	—	0.845	0.819	4.633
First-order	K^+	0.161	—	0.889	0.871	12.06
	NO_3^-	0.142	—	0.878	0.848	13.14
	HA	0.021	—	0.811	0.779	5.116
Higuchi	K^+	25.58	—	0.837	0.810	14.62
	NO_3^-	24.04	—	0.811	0.774	16.02
	HA	5.587	—	0.571	0.499	7.705
Korsmeyer Peppas	K^+	0.112	0.87	0.955	0.937	7.680
	NO_3^-	0.084	0.97	0.965	0.940	7.516
	HA	0.118	2.15	0.999	0.999	0.192

Swelling index of the prepared alginate beads. The swelling index of the prepared alginate beads was investigated by immersing 0.5 g of beads in 20 mL of water. The results are presented in Fig. 12. It is observed that the swelling index of the composite beads was 0.316 or 31.6% and was found to be saturated at 8 hours. The swelling rate is slower than usual due to the formation of denser beads in the presence of acid-activated biomass.[31] These slower swelling processes help in the long-term stability of the beads, making them ideal for the slower release of nutrients and ensuring long-term nutrient availability.[32] Further, the swollen beads release water gradually during the de-swelling process and assist in plant growth in arid regions.

Release of nutrients. Investigations were performed for the release of K^+, NO_3^- and HA from alginate beads, and the results are shown in Fig. 13. It is observed that the release of nutrients was slow and gradual for 2 weeks, and K^+ and NO_3^- leached 100%. The release of HA was found to be slow compared to the other two nutrients, and only around 35% was released over a span of 2 weeks. This is due to the complex structure of the HA molecule and polymer matrix hindering the release of HA. Further, the interactions of HA with ZnS nanoparticles and the biomass surface contribute to the slower rate of release. Although the K^+ and NO_3^- ions are not bound to the surface of the ZnS-AAB, and owing to their smaller ionic size, they tend to leach 100% compared to HA. These results suggest the ability of the composite alginate beads to apply seed coating in agriculture. The gradual release of the nutrients is consistent with the swelling index results observed earlier in this study.

Kinetics of the release of nutrients. The kinetic data of the nutrient release were analyzed with four kinetic models, such as zero order, first order, Higuchi and Korsmeyer and Peppas (K–P) models, and the respective plots and constants are presented in Fig. S3 and Table 7. As illustrated in Table 7, the zero-order and

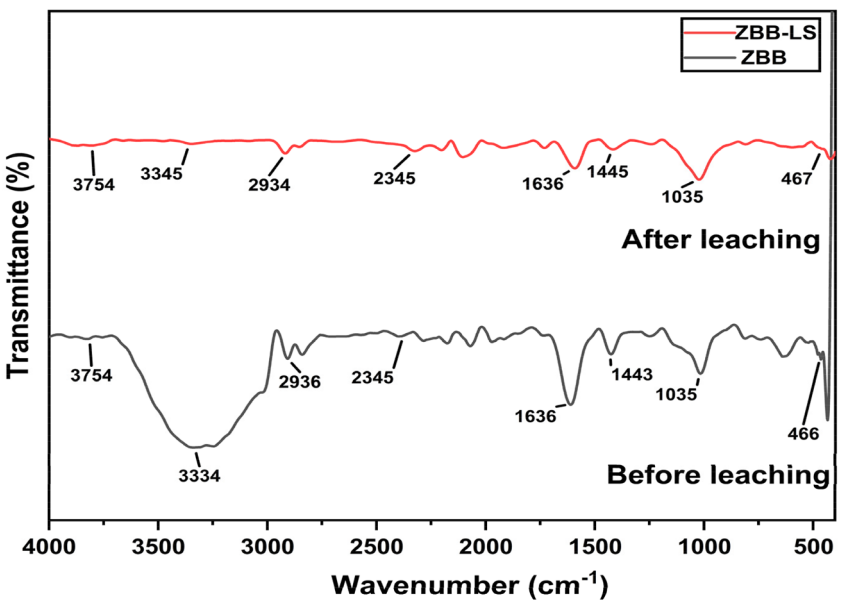

Fig. 14 FTIR spectra of HA-loaded ZnS-AAB alginate beads before and after the release of nutrients.

K–P models showed the highest correlation coefficients and low RMSE values, suggesting their ability to explain the release kinetics and mechanism of nutrient release from composite beads. The low correlation and high RMSE value of the first-order and Higuchi models suggest that there is less applicability of the models to the present system. The best fit of the zero-order model suggests that the release of nutrients follows a time-independent controlled release constant mechanism, which might be due to the swollen matrix of the beads.[33] The n values 0.87 and 0.97 from the K–P model suggest that the release of K^+ and NO_3^- ions is due to non-Fickian diffusion and relaxation-controlled transport of nutrients, which is in good agreement with zero-order observations.[34] A high n value of 2.1 obtained for HA is due to the complex interaction with ZnS-AAB; the swelling of the polymer matrix helps transport the HA molecule, and a high n value suggests that HA may rapidly burst release due to the degradation of the polymer beads.

Structural stability of beads. Structural stability of the beads after the release of nutrients was analyzed using FTIR and SEM techniques. The FTIR of ZnS-AAB alginate beads after release in comparison with fresh beads is presented in Fig. 14. It is observed that there are no significant changes in the functional groups observed in the post release beads compared to fresh beads, confirming that the alginate beads retain their structural integrity even after seven days of immersion in water. Additionally, SEM investigations were performed for the ZnS-AAB alginate beads to check any surface distortions or crack development during the water immersion period (Fig. 15a). It is observed that the structure of the beads was retained and that no cracks were observed on their surface. The EDX analysis (Fig. 15b) showed the absence of K^+ ions and the presence of all other elements, confirming the successful release of K^+ ions and the structural stability of the beads after the release of nutrients. These results suggest that the prepared beads were structurally stable for one week without any surface damage and were able

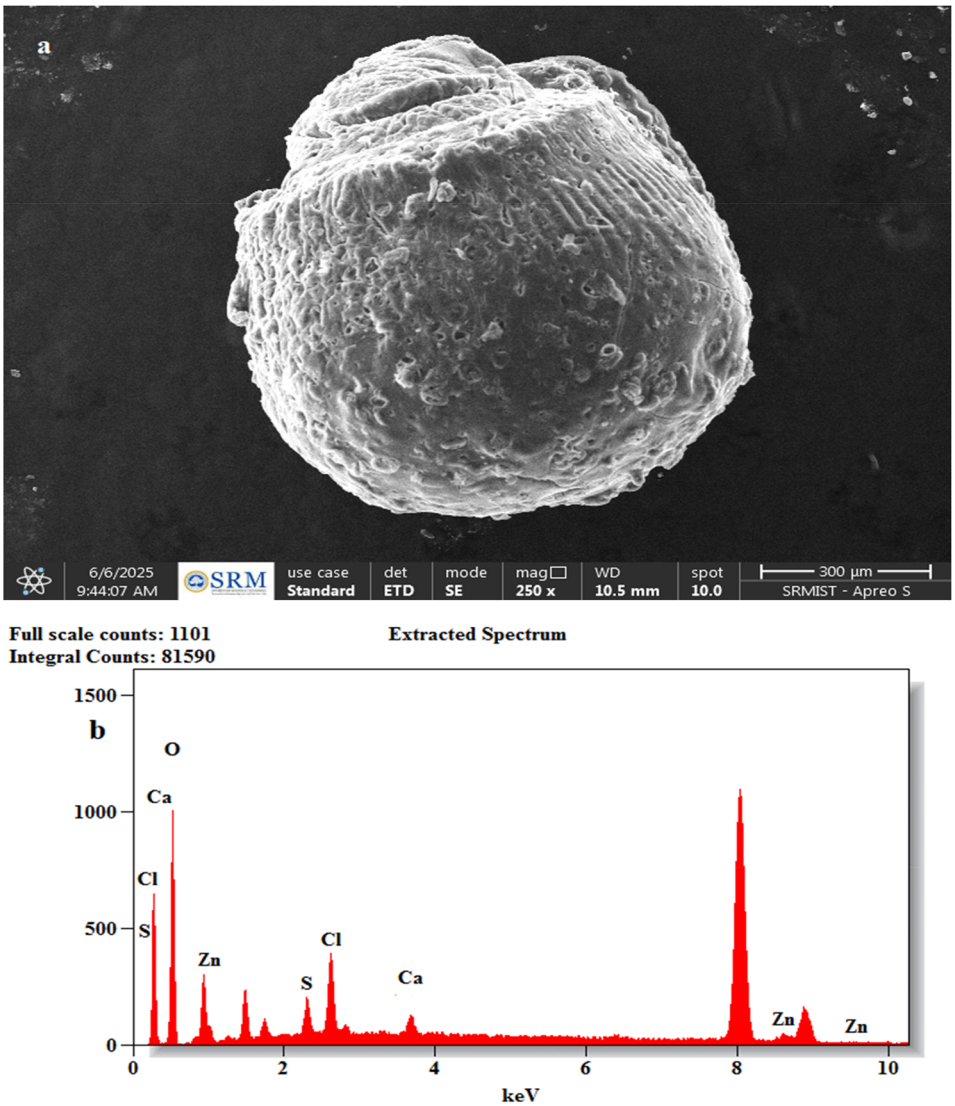

Fig. 15 (a) SEM image and (b) EDX pattern of ZnS-AAB alginate beads post nutrient release.

to release the nutrients successfully. This is in good agreement with the literature, where the alginate beads degrade slowly with respect to 1–2 weeks.[35–37] The structural stability exhibited by beads for one week in controlled environments indicates their suitability for nutrient release as proof of concept. However, their performance in soil environments and long term stability require further investigation before they are considered for real-time applications.

Environmental considerations and future directions. It is important to evaluate the environmental concerns of nutrient-loaded ZnS-AAB alginate beads since they are intended to be used in real-world applications. The gradual release of K^+ and NO_3^- ensures the optimal availability of the nutrients and avoids surface runoffs, which may later lead to eutrophication. The slow release of humic acid enhances soil health and microbes and further helps in water retention. The alginate beads prepared in this study are found to be stable in water for a week; later, they may break down and release the ZnS nanoparticles and biomass.[38] Since ZnS nanoparticles are immobilized on the biomass matrix, their direct release into the environment is minimized, reducing the risk of surface runoff and associated soil toxicity. Over time, microbial activity in soil can facilitate the gradual transformation of ZnS into bioavailable forms, such as Zn^{2+} and SO_4^{2-}, which can be utilized by plants as essential micronutrients. This controlled transformation supports sustained nutrient availability for plant growth.[39] The biomass is 100% biodegradable and exhibits no environmental impact, making the process sustainable and circular. However, if the ZnS nanoparticle degradation is too slow, it may affect the soil microbial community, accumulate in plants and exhibit toxicity. It is essential to evaluate the availability of a suitable microbial community that can potentially break down the ZnS nanoparticles in soil.[40] Hence, comprehensive long-term soil incubation and ecotoxicology studies are required to fully elucidate the environmental fate, bioavailability and safety of ZnS nanoparticles.

With the proof of concept, this study records that all the elements and molecules present in the ZnS-AAB alginate beads effectively support the plant growth system and contribute to sustainable products from waste. The circular economy is evident in the present approach, and it can be further improved by sourcing Zn and S from waste sources for the production of ZnS nanoparticles. Further, tailoring the alginate bead preparation depending on the soil type and plant variety would enhance the production quality. To close the loop of biomass, the biomass can be used in *Manilkara zapota* farming (zapota seeds – zapota seeds biomass beads – zapota soil), making the process circular and sustainable.

Conclusion

This study reports the first of its kind investigation on the adsorption of humic acid by ZnS nanoparticle-loaded biomass and its encapsulation in alginate beads for agricultural applications. The ZnS nanoparticles were green synthesized using *Manilkara zapota* seed extract, and the spent seeds were converted to biomass with acid activation. The synthesized ZnS nanoparticles were characterized using various analytical techniques and were found to be less than 2 nm in size with no specific shapes. The presence of ZnS nanoparticles on AAB is confirmed by FTIR spectroscopy, XRD, SEM and EDX techniques. The adsorption of humic acid onto ZnS-AAB was optimized using the BBD of the RSM. The design was found to be significant and reliable with a p-value of 0.0001, and the correlation coefficients of experimental, adjusted and predicted are close to one. Isotherm and kinetic investigations highlighted the applicability of the models to equilibrium and kinetic data. However, the error analysis provided much more evidence on the better applicability of Langmuir and pseudo second order kinetic models to the experimental data. A mean free energy value of 12.45 kJ mol^{-1} obtained for the D-R isotherm and an activation energy of 24.5 kJ mol^{-1} obtained from the Arrhenius equation affirm the physical adsorption of humic acid onto ZnS-AAB. The thermodynamic investigations further support the spontaneity and exothermic nature of adsorption, and the enthalpy value supports the physical adsorption of the present process. The humic acid-loaded ZnS-AAB was encapsulated into alginate beads with the addition of K^+ and NO_3^- ions to make the entire adsorption process sustainable. The successful encapsulation of all the ions and humic acid-loaded ZnS-AAB was evidenced by EDX analysis. The beads were initially investigated for their swelling index and found to be 31% for 8 hours. The swelling is found to be a slow process due to the presence of biomass, which assists in water retention for a longer time. The release of nutrients was found to be in the order of $K^+ > NO_3^{2-} >$ HA depending on the size of the ions and molecules. The beads were found to be stable even after a week of immersion in water, making them suitable for practical application in agriculture for the controlled supply of macro and micro nutrients. The results demonstrate that the present process is sustainable and circular from waste to wealth, with specific agricultural applications.

Author contributions

JB: investigation, formal analysis, manuscript writing; RL: conceptualization, supervision, data analysis, manuscript review and editing.

Conflicts of interest

Authors declare no conflicts of interest.

Data availability

The data supporting this article have been included as part of the supplementary information (SI). Supplementary information is available. See DOI: https://doi.org/10.1039/d6ra00928j.

Acknowledgements

The authors acknowledge the SCIF and NRC of SRM Institute of Science and Technology for the instrumental characterization support.

References

1 Y. Li, F. Fang, J. Wei, X. Wu, R. Cui, G. Li, F. Zheng and D. Tan, *Sci. Rep.*, 2019, **9**, 12014.
2 S. D. Richardson and C. Postigo, *Emerging Organic Contaminants and Human Health*, 2011, pp. 93–137.
3 Y. Zhan, Z. Zhu, J. Lin, Y. Qiu and J. Zhao, *J. Environ. Sci.*, 2010, **22**, 1327–1334.
4 M. Habuda-Stanić, A. Tutić, D. Kučić Grgić, A. Zeko-Pivač, A. Burilo, S. Paixão and M. Šiljeg, *Chem. Biochem. Eng. Q.*, 2021, **35**, 189–203.
5 H. Yu, Q. Zhang, M. Dahl, J. B. Joo, X. Wang, L. Wang and Y. Yin, *Chemistry*, 2017, **23**, 16249–16256.
6 S. Gueu, G. Finqueneisel, T. Zimny, D. Bartier and B. K. Yao, *Adsorpt. Sci. Technol.*, 2019, **37**, 77–94.
7 L. Wang, D. D. Dionysiou, J. Lin, Y. Huang and X. Xie, *Chemosphere*, 2021, **279**, 130491.
8 S. P. Moussavi, A. Kadier, R. Singh, R. Ashoori, M. Shirinkar, J. Lu, N. S. Zaidi and F. Sher, *Chemosphere*, 2022, **301**, 134673.
9 N. Pourbakhsh, H. Hazrati and S. Gharibian, *Int. J. Environ. Sci. Technol.*, 2025, **22**, 6557–6572.
10 T. Alomar, H. Qiblawey, F. Almomani, R. I. Al-Raoush, D. S. Han and N. M. Ahmad, *J. Water Process Eng.*, 2023, **53**, 103679.
11 A. Naghizadeh, F. Momeni, E. Derakhshani and M. Kamranifar, *Desalin. Water Treat.*, 2017, **100**, 116–125.
12 A. Naghizadeh, H. Shahabi, F. Ghasemi and A. Zarei, *J. Water Health*, 2016, **14**, 989–997.
13 S. Ouni, A. Madaci, M. Haouari, *et al.*, *J. Inorg. Organomet. Polym.*, 2023, **33**, 2574–2585.
14 M. Bhushan, R. Jha and R. Bhardwaj, *J. Phys. Chem. Solids*, 2019, **135**, 109021.
15 A. Al-Sharabi, A. Alnehia, A. H. Al-Hammadi, *et al.*, *J. Inorg. Organomet. Polym.*, 2022, **33**, 20812–20822.
16 R. Lakshmipathy, M. K. Kesarla, A. R. Nimmala, S. Godavarthi, C. M. Kukkambakam, L. M. Gomez and N. C. Sarada, *Res. Chem. Intermed.*, 2017, **43**, 1329–1339.
17 F. A. La Porta, J. Andres, M. S. Li, J. R. Sambrano, J. A. Varela and E. Longo, *Phys. Chem. Chem. Phys.*, 2014, **16**, 20127–20137.
18 M. M. H. Farooqi and R. K. Srivastava, *Mater. Sci. Semicond. Process.*, 2014, **20**, 61–67.
19 M. R. Vipin and U. Shanker, *Biomass Convers. Biorefin.*, 2025, **15**, 3941–3963.
20 A. Bülbül, A. Delibaş and R. Coşkun, *Biomass Convers. Biorefin.*, 2025, **15**, 23227–23242.
21 M. Rajkumar, S. I. D. Presley, F. Menaa, *et al.*, *Bioprocess Biosyst. Eng.*, 2024, **47**, 2111–2129.
22 V. V. Devi, L. R, V. P. Sundramurthy, D. Ali, S. Alarifi and M. Sillanpaa, *Chem. Eng. Commun.*, 2025, **212**, 50–63.
23 G. T. Elakkiya, G. Sundararajan, R. Lakshmipathy, P. Anitha and N. Muruganantham, *Bull. Chem. Soc. Ethiop.*, 2024, **38**, 631–645.
24 K. Chen, Q. Feng, Y. Feng, D. Ma, D. Wang, Z. Liu and J. Feng, *Chem. Eng. J.*, 2022, **435**, 135171.
25 S. Gupta, A. Prajapati, A. Kumar and S. Acharya, *Watershed Ecol. Environ.*, 2023, **5**, 241–254.
26 A. Hsini, Y. Naciri, M. Benafqir, Z. Ajmal, N. Aarab, M. Laabd and A. Albourine, *J. Colloid Interface Sci.*, 2021, **585**, 560–573.
27 M. Masuku, J. F. Nure, H. I. Atagana, N. Hlongwa and T. T. Nkambule, *J. Environ. Manage.*, 2025, **373**, 123705.
28 A. El Idrissi, O. Dardari, F. N. N. N. Metomo, Y. Essamlali, A. Akil, O. Amadine and M. Zahouily, *Int. J. Biol. Macromol.*, 2023, **253**, 127229.
29 K. Ampong, M. S. Thilakaranthna and L. Y. Gorim, *Front. Agron.*, 2022, **4**, 848621.
30 N. Wang, B. Wang, Y. Wan, B. Gao and V. D. Rajput, *J. Environ. Manage.*, 2023, **348**, 119133.
31 S. Popov, N. Paderin, D. Khramova, E. Kvashninova, O. Patova and F. Vityazev, *Int. J. Mol. Sci.*, 2022, **23**, 3388.
32 M. S. Haydar, D. Ghosh and S. Roy, *Plant Nano Biol.*, 2024, **7**, 100058.
33 I. S. Bayer, *Pharmaceutics*, 2023, **15**, 1364.
34 M. Szekalska, M. Wróblewska, K. Sosnowska and K. Winnicka, *Int. J. Polym. Sci.*, 2016, **2016**, 8635408.
35 M. L. Moya, M. Morley, O. Khanna, E. C. Opara and E. M. Brey, *J. Mater. Sci.:Mater. Med.*, 2012, **23**, 903–912.
36 N. K. D. Devi, M. Chandana, A. Sindhura, G. Ratnavali and R. Kavitha, *Pharmacophore*, 2010, **1**, 196–213.
37 B. Wang, Y. Wan, Y. Zheng, X. Lee, T. Liu, Z. Yu and B. Gao, *Crit. Rev. Environ. Sci. Technol.*, 2018, **49**, 318–356.
38 N. Wang, B. Wang, Y. Wan, B. Gao and V. D. Rajput, *J. Environ. Manage.*, 2023, **348**, 119133.
39 V. Khepar, A. Sidhu and S. Chandel, *Environ. Res.*, 2024, **251**, 118624.
40 E. Hidayat, N. M. M. Sarbani, S. Samitsu, F. A. A. Nugroho, S. K. Lahiri, M. Aoyagi and H. Harada, *Arabian J. Chem.*, 2024, **17**, 105877.